Available online at www.scholarsresearchlibrary.com

Scholars Research Library

Scholars Research Library

Archives of Applied Science Research, 2018, 10 (2): 12-26

(http://www.scholarsresearchlibrary.com)

ISSN:0975-508X

Solvent free transesterification of ethylacetoacetate and higher alcohols over nanocrystalline CeO_2 loaded hierarchical Mobil Five (MFI) zeolite

Mithun Nandi*

Department of Chemistry, Gauhati University, Guwahati, Assam, 781014, India

ABSTRACT

Considering the importance of efficient and greener transesterification of ethylacetoacetate to ß-keto esters we employed a top-down method of synthesis of hierarchical MFI supported CeO_2 for green protocol. The catalyst was characterized by different techniques such as powder X-ray diffraction (XRD), Fourier-transformed infrared spectroscopy (FTIR), thermo gravimetric analysis (TGA), scanning electron microscopy (SEM), transmission Electron microscopy (TEM), nitrogen adsorption-desorption, UV-vis diffused reflectance spectroscopy and X-ray photoelectron spectroscopy (XPS) methods. The CeO2 supported MFI was evaluated for the transesterification of ethyl acetoacetate by n-amyl alcohol. The influence of temperature and time, molar ratio, catalyst amount and hierarchical topology of MFI on the reaction was investigated. The catalyst exhibited efficient heterogeneous catalytic activity for the transesterification of ethyl acetoacetate and n-amyl alcohol with 97% conversion at 4 h of reaction time under the optimised reaction temperature. A second order kinetics was observed for the reaction with activation energy of 43.8 kJmol-1. The catalyst was also found to be effective for linear long chain, aryl, cyclic and tertiary alcohols as well. The heterogeneous reaction was adopted avoiding the use of any solvent. Reuse of the catalyst for at least five consecutive runs did not show any significant activity.

Keywords: MFI, hierarchical MFI, ceria, ß-keto esters, transesterification

HIGHLIGHTS

Ceria loaded on hierarchical MFI (CeAM) is a novel catalyst that has not yet been explored to the best of our knowledge, although advantages of hierarchical nature of MFI has recently been exploited for oxidation of styrene to benzaldehyde.

CeAM shows excellent catalytic activity (in terms of both conversion and selectivity) for the transesterification of ethyl acetoacetate under mild reaction conditions which can be attributed to a combined effect of the electron withdrawing nature and hierarchical topology of the catalyst.

The present investigation was carried out without the use of any solvent which not only brings down the use of expensive solvents but also provides a green synthetic route.

Graphical Abstract

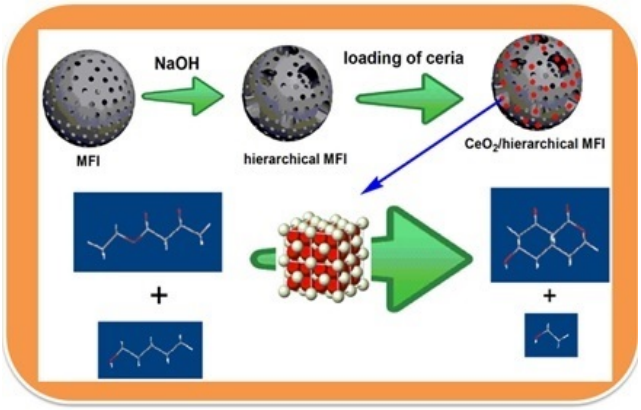

INTRODUCTION

Transesterification in recent times is a widely studied reaction in association with the fabrication of fuels and chemicals from renewable feed stocks. Transesterification of vegetable oil with alcohols has long been a preferred method for the production of biodiesel [1] and in several industrial processes such as co-synthesis of dimethyl carbonate and ethylene glycol [2], polyethylene terephthalate from dimethyl terephthalate and ethylene glycol [3]. β-keto esters are significant classes of intermediates that are widely used in pharmaceuticals, agrochemicals and dyestuff industries. They are also among the basic building blocks for the synthesis of many natural products, additives for paints and pheromones. β-keto esters being the closest structural analogs of β-diketones, are also found to exhibit antiviral activity [4]. Various synthetic methods that involve both homogeneous and heterogeneous catalysts, strong acids, metal salts, amine, titanosilicates and soluble base catalysts have been reported for the synthesis of β-keto esters [5]. Owing to the corrosive and toxic properties of homogenous catalysts, much importance have been shifted in recent times for employing heterogeneous catalytic methods that has many advantages including easy separation of the catalyst and reusability. Mesoporous carbon encaptulated with SrO had also been employed for the transesterifiaction of ethyl acetoacetate [6]. Anand et al. [7] studied the transesterification of ethyl acetoacetate with metal free mesoporous carbon nitride. The basicity of the active sites vis-a-vis benefit of mesoporous nature of the catalysts was clearly reflected in their catalytic activity. AgOtf and other Ag(I)-based catalytic system were reported to be active for the transesterification of EAcA and many functionalized alcohols smoothly [8]. A similar active catalyst, Niobium (V) oxide has also been reported to achieve good conversion and moderate to good isolated product yields [9]. Unfortunately, the above mentioned systems involve the usage of highly toxic and expensive solvents at elevated temperatures and longer reaction time. Therefore, the development of an environmentally benign, highly active catalyst that would curtail the reaction time and temperature and could be reused without being leached is still being investigated. It is well documented that the basicity of rare earth metal oxides are more advantageous than that of alkali and alkaline earth metal oxides for transesterification reactions [10]. Among the rare earth elements in the earth's crust cerium is the most abundant (66.5 ppm) which is similar or even more abundant than that of copper and tin [11]. The catalytic activity of CeO_2 is closely related to the energy of oxygen vacancy formation on the surface of ceria. Cerium oxides are also good oxygen buffers due to their redox capability [12]. These oxides have been found to be effective for a number of organic transformations such as dimerization of alcohols, alkylation of aromatic compounds, cyclization of diols and many others [13]. For a heterogeneous catalyst, support acts as a vehicle for the active phases and also for promoters. As documented by Bond [14], support facilitates the development of extremely small particles having maximum proportion of their active sites on the surface and also enhances the thermal and mechanical stability of the catalyst. Zeolite provides a wide spectrum of application in adsorption, catalytic and ion exchange properties based on their microporous nature. However, the sole microporous nature of zeolites imposes limitations due to pore size constraints involving relatively large size molecules especially for petrochemicals, pharmaceutical or fine chemical synthesis [15]. Different types of mesoporous molecular sieves and amorphous silica in the early 1990s were able to overcome this limitation to some extent but the excitement was tempered due to their lower crystallinity, thermal and mechanical stability. Hierarchical MFI alleviates the above mentioned drawbacks by coupling the intrinsic microporosity with secondary mesopore network of inter- or intracrystalline nature [16]. An investigation was carried out in one of our earlier reported works where a simple and economic process of alkali treatment were utilised for mesopore formation in MFI [17]. The results clearly showed the hierarchical topology of the samples with increased mesopore volume and somewhat

decreased micropore volume. The advantage of enhanced mesoporosity of MFI in the catalytic etherification of glycerol was also clearly depicted by Camino et al. [18]. Ogunronbi et al. [19] also developed Ga containing hierarchical MFI and reported better result as compared to the parent MFI loaded moiety for the aromatization of propane. Recently, we have reported the better catalytic performance of vanadia and ceria-zirconia solid solution loaded on hierarchical MFI than that loaded on parent MFI for oxidation of cyclohexene [20] and ethyl benzene [21] respectively. To the best of our knowledge the activity of ceria supported on hierarchical MFI in the transesterification of ethyl acetoacetate with higher alcohols had not yet been explored. We expect that hierarchical nature of MFI with composite network of micro and mesopores would serve as an excellent support for loading of ceria.

In this present work, we report the activity of ceria introduced hierarchical MFI for the transesterification of ethyl acetoacetate and n-amyl alcohol under heterogeneous reaction conditions. The effect of various parameters such as temperature, molar ratio of reactants, catalyst amount and reaction time was monitored for this reaction. The catalyst has also been tested for transesterifying linear long chain, cyclic, aryl and tertiary alcohols to the corresponding β-keto esters. The kinetics of the reaction with n-amyl alcohol was monitored to determine the rate constant and activation energy and a schematic mechanism has been proposed. A green route for the reaction was followed by avoiding the use of any solvent and recycling the catalyst for at least five consecutive runs without noteworthy loss of its catalytic activity.

EXPERIMENTAL PROCEDURES

Catalyst preparation

Parent MFI with silica to alumina ratio (SAR) 100 was synthesized by hydrothermal technique following our previously reported novel method [22]. The calcined product (designated as PM) was modified by alkali treatment using 0.4 M NaOH solution. To 150 mL of 0.4 M NaOH solution pre-heated at 343 K in a polyethylene beaker was placed in a water bath, 2g of PM was added and stirred at that temperature for 60 minutes. The beaker was immediately placed in an ice-bath to avoid further reaction and the suspension was filtered and washed several times with distilled water until all the alkali was removed. The filtered product was dried overnight (12h) at ambient temperature and then at 383 K in an air oven for 6h. The resulting alkali treated sample is designated as AM and is shown schematically in Scheme 1. To prepare hierarchical MFI supported ceria nanocatalyst (CeAM), the deposition of $(NH_4)_2Ce(NO_3)_6$ complex onto AM surface was performed by wet impregnation technique. Calculated amount of the complex was dissolved in minimum volume of ethanol with the simultaneous addition of vaccum dried AM support (383 K, 6h) and stirred at room temperature for 2h. The solution was then allowed to evaporate at ambient temperature and dried at 383 K for 6h. Finally the sample was calcined at 773 K to favour complete crystallization of the fluorite structure of ceria [23].

Scheme1. Alkali treatment of parent MFI zeolite

Catalytic transesterification of ethyl acetoacetate

Liquid phase transesterification of ethyl acetoacetate and n-amyl alcohol was carried out in a 25 mL round bottomed flask placed in a sand bath and equipped with a reflux condenser. The reaction was optimized for different parameters such as molar ratios of the reactants, amount of catalyst and reaction time in the temperature range 313-343 K maintaining the total volume of reactants at 5 mL for each run. The catalyst was preheated at 383 K for 4h before use. Reaction mixture withdrawn after specific intervals of time was analyzed by Gas Chromatography (Bruker 430 GC) fitted with WCOT fused silica 30 m × 0.32 mm column and FID detector.

Characterization of samples

Powdered X-ray diffraction patterns were recorded on a Bruker D-8 Advance X-ray Diffractometer operated at 40 kV and 40 mA using Cu Kα radiation of wavelength 0.15418 nm for phase identification and to determine the crystallite size and crystallinity. The XRD data were collected in 2θ range 5-50^{o}(step size 0.05^{o} and step time 0.5s). IR spectra were recorded on KBr discs in a Perkin Elmer RX1 spectrophotometer in the mid-IR range of 2000-450 cm^{-1} to complement the XRD results. Surface morphological study was carried out by a SIGMA VP (ZEISS) scanning electron microscope at an accelerating voltage of 5 kV. Elemental analysis was carried out with the help of Carl Zeiss SIGMA VP using EHT 20 kV EDX. Hitachi 4100 spectrometer equipped with a diffuse reflectance attachment was used to record the diffuse reflectance UV-vis spectra of the solid catalysts in the range 200-800 nm. Transmission electron microscopy (TEM) pictures were recorded on a JEOL 2011 electron microscope. The thermal stability of all the catalysts were studied by thermal gravimetric analysis technique using Mettler Toledo TGA/DSC 1, STARe System Analyser in the temperature range 313-1173 K applying a heating rate of 10 min-1 under a nitrogen gas atmosphere. The nitrogen adsorption-desorption study of the samples were done by MicromeriticsTristar 3000 analyzer. Prior to the surface area analysis all the samples were degassed by passing a constant flow of nitrogen at 473 K for 6h to remove any adsorbed gases. XPS study was carried out by PHI Quantum 5800 ESCA X-ray photoelectron spectroscopy equipped with a microfocussing Al Kα as X-ray source.

RESULTS AND DISCUSSION

X-Ray diffraction

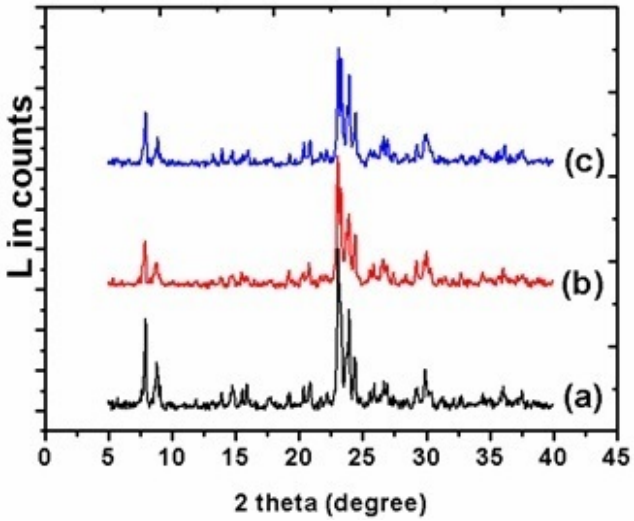

Figure 1. XRD pattern of (a) PM (b) AM (c) CeAM

The X-ray diffraction pattern of parent MFI (Figure 1a) shows prominent peaks in the range 2θ = 7-9^{o} and 23^{o} that corresponds to specific peaks for MFI indicating formation of pure MFI phase 24. On alkali treatment up to 60 min it is observed that the basic structure of MFI remains intact with a nominal decrease in the intensity of the prominent peaks. The decrease can be attributed to extraction of silicon from zeolite framework. No reflections pertaining to ceria could be resolved in the XRD pattern of CeAM (Figure 1c) indicating that ceria species exist as highly dispersed extra nanocrystalline oxides on the zeolite surface [19]. The crystallite size was calculated from Williamson-Hall plot (Figure 2). The simplified equation is,

$$\beta\cos\theta = \frac{K\lambda}{D} + 4\varepsilon sin\theta$$

where, β is the line broadening at half the maximum intensity (FWHM) in radian, D is average crystallite size, θ is Bragg angle in radian, K is a dimensionless shape factor close to unity, λ is the wavelength of the X-ray and ε is the average strain. The crystallite size and strain is achieved from the intercept and slope of the linear fit respectively by plotting a graph between 4sinθ and βcosθ. Upon alkali treatment the crystallinity of the the parent MFI decreased from 98% to 92% as evaluated from the (101) and (501) reflections using the following relation,

$$\%C = \frac{I_{hkl}}{I_b + I_{hkl}}$$

for a particular crystallographic plane (hkl) where, Ib is the integral background intensity and Ihkl is the integral peak intensity with reference to (101) and (501) reflections. The crystallite size and crystallinty of the samples are presented in Table 1.

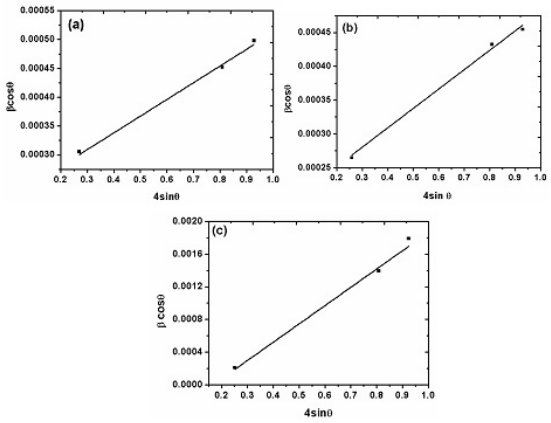

Figure 2. Williamson-Hall plot for (a) PM (b) AM (c) CeAM

Table 1. Crystallite size and crystallinity of the prepared samples from XRD analysis

Entry	Samples	Crystallite size (nm)	R^2	(%C)[1]501,101from XRD
1	PM	46	0.97	98
2	AM	42	0.94	92
3	CeAM	43	0.92	95

Infrared Spectroscopy

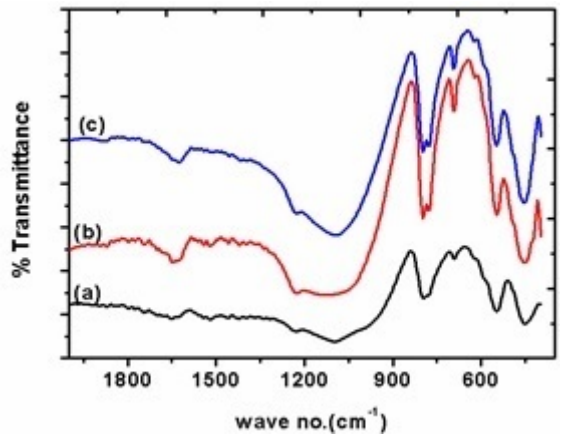

Figure 3. FT-IR spectra of (a) PM (b) AM (c) CeAM

Figure 3 depicts the FTIR transmission spectra of the parent and modified MFI samples (AM and CeAM). FTIR spectra of PM closely resembles to that of previously reported IR spectra of MFI supporting formation of pure phase of MFI [25]. The transmission spectra of the desilicated and ceria loaded sample also seems to exhibit absorbance bands similar to that of parent MFI showing prominent absorbance bands at around 1090 (internal asymmetric stretching), 1229 (external asymmetric stretch), 794 (external symmetric stretch), 550 (double ring vibration) and 450 cm^{-1} (T-O bending). However, the gradual shift of the band around 1090 cm^{-1} towards lower wavelength and enhancement of absorbance bands around 794 and 450 cm^{-1} for AM is most likely due to the loss of Si from PM framework17. This complements the results obtained from XRD analysis. The decrease of the band near 550 cm^{-1} is

a reflection of the lowering of crystallinity [26]. The further alteration in intensity of the absorbance bands near 794 cm^{-1} and broadening in the T-O-T internal asymmetric stretch region around 1090 cm^{-1} for CeAM suggests loading of hetero atom on AM [27].

UV-Vis DR Spectra

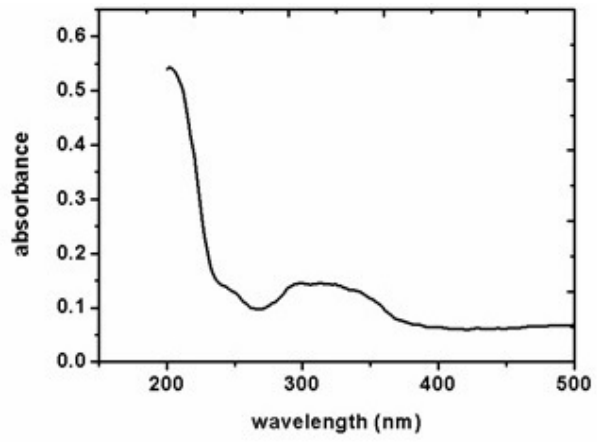

Figure 4. UV-vis DRS of CeAM

The room temperature UV-vis DR spectra of CeAM is depicted in Figure 4. Basically literature suggests two absorption bands for ceria at around 280 and 410 nm [28]. However, the band positions strongly depends upon the ligand field symmetry of the central Ce, temperature, types of ligands, medium and several such other factors. The well-defined single broad absorption band observed in the range 270-365 nm suggests the charge transfer from ligand to metal i.e Ce_4+(4f) ← O_2-(2p) as reported previously [29]. This is further complemented by the XPS analysis. Bensalem et al accounted the broadening of this peak as due to increasing number of surface defects [30]. The existence of this broad band centred around 320 nm without the absorption at higher wavelength (410 nm) as observed in our case may be due to the presence of large amount of Ce in tetrahedral environment [29]. The 4d-5f transition in the 220-250 nm range that occurs predominantly in the UV region [31] can be attributed to the presence of some isolated surface Ce^{3+}.

Thermo gravimetric analysis

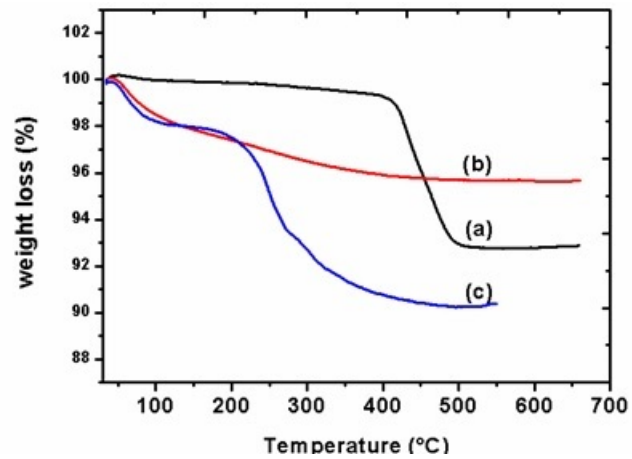

Figure 5. TGA curves of (a) PM (b) AM (c) CeAM

The initial weight loss up to 423 K for all the samples (Figure 5a) resulted from desorption of water. The loss during 373-423 K can be attributed to desorption of occluded water. The mass loss in the temperature range 423-773 K for the parent uncalcined MFI is due to desorption of tetrapropylammonium bromide (template) used during the synthesis, while beyond 773 K the rate of mass loss is insignificant. Round et al [32] well documented this mass loss due to desorption of four types of tetrapropylammonium (TPA^+)cations. AM shows a weight loss in the broad

temperature range 373-1073 K which is possibly due to the removal of sodium hydroxide (Figure 5b). Since the hierarchical MFI was calcined previously so no breakdown due to loss of organic template is observed. The prominent breakdown for CeAM in the region 383-673 K can be attributed to the following set of reactions related to the decomposition of Ce(IV)$(NH_4)_2(NO_3)_6$ passing through double valence change of cerium [33].

$$Ce(IV) \rightarrow Ce(III) \rightarrow Ce(IV).Ce(IV)\left(NH_4\right)_2\left(NO_3\right)_6 \rightarrow \frac{1}{3}Ce(III)2\left(NH_4\right)_3\left(NO_3\right)_9 + \frac{1}{3}CeO_2 + \left(NH_3, NO, NO_2, O_2\right) \quad (388 - 523\,K)$$

$$\frac{1}{3}Ce(III)2\left(NH_4\right)_3\left(NO_3\right)_9 \rightarrow \frac{2}{3}CeO_2 + \left(NH_3, NO, NO_2, O_2\right) \quad (523 - 673\,K)$$

SEM-EDX spectrum

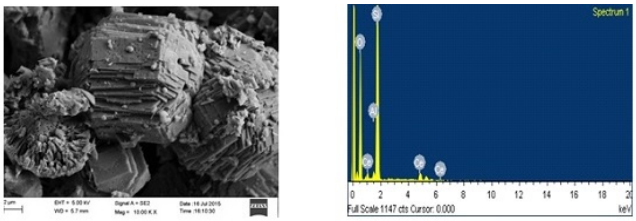

Figure 6. SEM image and EDS of CeAM

Figure 6 demonstrates the SEM micrographs of CeAM. From SEM analysis it is seen that the particles exhibit cuboidal shape and size of around 10 μm. Some agglomeration of the particles as observed from SEM micrograph may be due to the tendency of ceria to lower the surface energy [34]. The cracks and faults observed is possibly due to alkali treatment of parent MFI that might involve the breakage of intracrystalline Si-O-Si and Si-O-Al bonds, as reported in our earlier work [17]. The elemental composition of the sample as obtained from the energy dispersive spectroscopy (EDS) confirms the even distribution of Ce, Al, Si and O in the material (Figure 6). The practical weight percentage of Ce is found to be in good agreement with our expected value (Table 2).

Table 2. Chemical composition of CeAM as calculated from EDS analysis

Element	Atomic (%)
O K	73.17
Na K	1.08
Al K	0.27
Si K	24.32
Ce L	1.16

Totals	100

Transmission Electron Microscopy

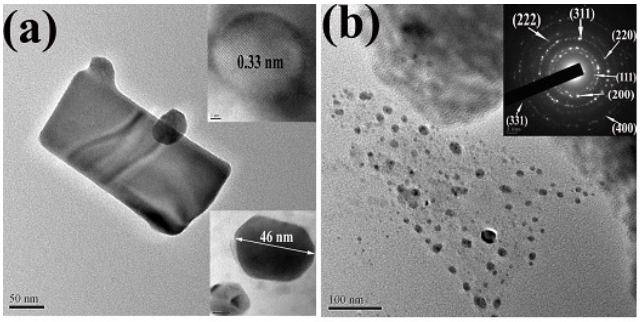

Figure 7. TEM image showing (a) lattice fringe and crystallite size (b) distribution and SAED (inset) of CeAM.

The TEM image (Figure 7a) reveals the co-existence of two types of crystals, the bigger one may be predominantly of hierarchical MFI zeolite and the comparatively smaller one supported on the bigger crystals are due to ceria. The selected area diffraction pattern is the projection of the reciprocal lattice with lattice reflection showing as diffraction spots and each spot arising from Bragg reflection from an individual crystallite. It gives information about the crystallinity of a sample and more specifically about the electron diffraction pattern from a selected area. The different diffused rings (Figure 7b, inset) could be assigned to (111), (200), (220), (311), (222), (400), (331) reflections of fcc lattice and fluorite structure of ceria [35]. The well-ordered ring pattern confirms polycrystalline nature of the sample. The admirable bright spots reveal high crystallinity of the material and complements the XRD data. The HRTEM image of a single crystallite (Figure 7a, inset) obtained by focussing the electron beam on a ceria crystallite lying on the TEM grid shows a hexagonal profile for CeO_2. The high-resolution lattice fringe (Figure 7a, inset) shows the reticular lattice planes inside the crystallite and these planes are continuously extended to the whole particle without any faults or twins. The measured inter planar lattice fringe is found to be 0.33 nm which corresponds to (111) reflection of CeO_2 [36]. Figure 7b shows the uniform dispersion of ceria crystallites with a narrow range of particle size. The histogram shows the particle size distribution between 45-48 nm centred around 45 nm (Figure 8).

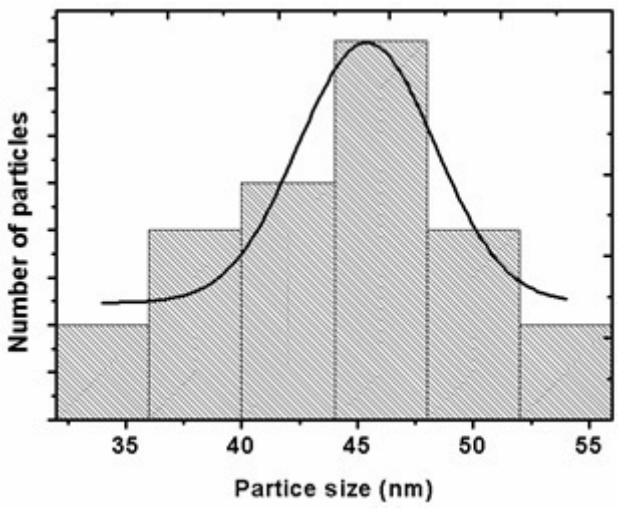

Figure 8. Particle size distribution for CeAM

Surface Area Analysis

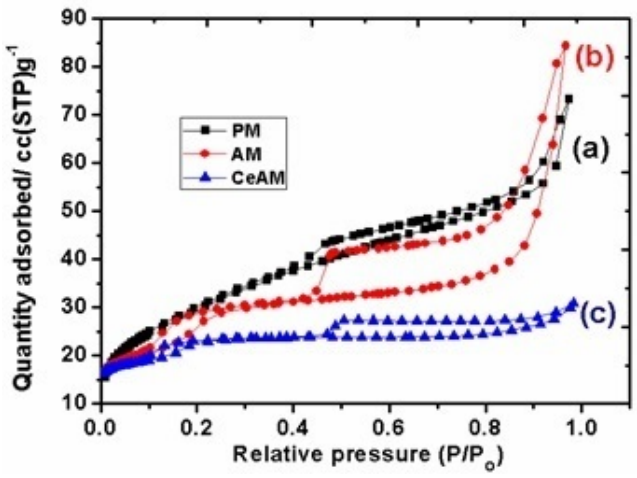

Figure 9. Nitrogen adsorption-desorption isotherm of (a) PM (b) AM (c) CeAM

Figure 9 illustrates the nitrogen adsorption-desorption isotherm of the parent and modified MFI samples (AM and CeAM). PM exhibits a type1 isotherm with high up taking at relatively low pressure indicating its microporous nature [37]. The isotherm of the modified samples shows the presence of hysteresis loop along with capillary condensation suggesting the presence of mesopore structure [38]. A bimodal pore system is observed for hierarchical MFI and CeAM sample, signifying the presence of two types of mesoporosity. The capillary condensation at lower p/pO∼0.2-0.4 can be attributed to the mesoporosity confined in the framework and the second loop observed in the desorption branch at higher partial pressure indicates the existence of mesoporosity arising due to intercrystalline voids in the crystal arrangement [39]. Although alkaline treatment leads to subsequent generation of mesopores, the sample microporosity still prevails as could be evidenced from the high nitrogen uptake of the samples at relatively low pressure. The alkali treated samples exhibit isotherm representing combined type I and type IV behaviour with pronounced hysteresis loops. BET surface area of the parent sample increased from 396.78 m_2/g to 439.62 m_2/g upon alkali treatment for a duration of 60 min. In a similar way, alkali treatment of parent MFI showed a significant increase in the mesopore volume from 0.06 to 0.25 cm_3g^{-1} with a marginal drop in the micropore volume. Derived textural property reveals that there is a reduction in the surface area and micro and mesopore volume upon impregnation of ceria, which may be due to partial blockage of the pore mouths with the formation of nano crystalline CeO_2 aggregates.

Table 3. Textural and structural properties of parent and modified MFI samples

Physical properties	**Samples**		
	PM	**AM**	**CeAM**
BET surface area (m2g-1)	396.78	439.62	371.65
Micropore volume (cm3g-1)	0.16	0.12	0.07
Mesopore volume (cm3g-1)	0.06	0.26	0.19
BJH desorption cumulative pore volume (cm3g-1)	0.15	0.19	0.16

XPS analysis

XPS analysis of CeAM is carried out to identify the chemical states of the elements present by comparing the photoelectron binding energies with that of previously reported results. The full surface survey (Figure 10a) illustrates the presence of different elements on the surface of AM and reveals the presence of surface states of the metal with oxygen vacancies. The 3d XPS spectra of ceria is found to be composed of eight peaks and assigned as shown in Figure 10b. The spin-orbit components 3d3/2 and 3d5/2 are designated as u and v respectively. The peaks corresponding to u (ca. 902.47 eV), u" (ca. 905.97 eV) and u"' (914.83 eV) results from Ce4+ 3d3/2 while the peaks at v (880.95 eV), v" (887.92 eV) and v"' (897.15 eV) results from Ce4+ 3d5/2. The peaks assigned as u' (ca. 885.71

eV) and v' (ca. 904.3 eV) corresponds to Ce40 in Ce3+. The XPS analysis of the material reveals the chemical valence of Ce in mainly +4 oxidation state with a minor amount of Ce3+ and is found to be in parity with the UV-DRS analysis. The O 1s XPS spectra of ceria is depicted in Figure 10c. It clearly shows two distinct surface oxygen species representing the primary O 1s ionization and chemically shifted O 1s from chemisorbed surface species. The prominent lowest binding energy peak at 530.47-53.15 eV (O') is attributed to the typical lattice oxygen bonding to cerium ions while the shoulder peak at relatively higher binding energy 534.35-53.55 eV (O'') is assigned to defective or adsorptive oxygen species [39].

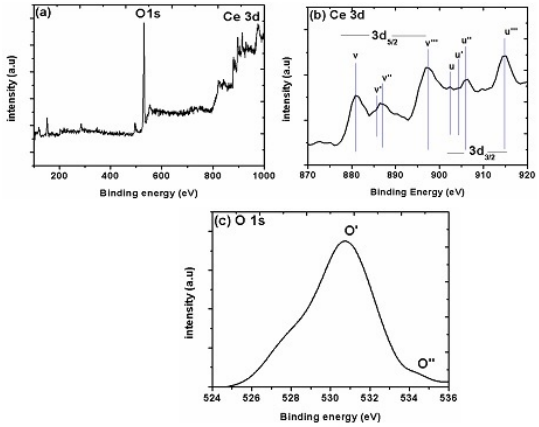

Figure 10. (a) XPS full survey (b) XPS survey for Ce 3d and (c) XPS survey for O 1s of CeAM

Catalytic activity

Initially a blank reaction (without catalyst) was carried out with 1:2 molar ratio of EAcA : n- amyl alcohol at 343 K for 6h but negligible amount of conversion was observed. The reaction was also tested at room temperature using 0.1 g of the catalyst and molar feed ratio of 1:2 for 6h, but no conversion was observed. In order to study the effect of temperature the reaction was then carried out in the temperature range 313-343 K with same molar ratio and 0.1 g of catalyst. The conversion enhanced from 38 to 97 % with the rise in temperature from 313 to 343 K at 4h of reaction time (Table 4). At higher temperature as the available activation energy for a reaction increases, so the reaction became faster at 343 K compared to 333 K and other lower temperatures. To understand the nature of CeAM towards the transesterification of EAcA with time, the progress of the reaction was monitored and analysed after definite intervals of time at different temperatures and results are presented in Figure 11.

It is observed that the conversion increases by about 10% on increasing the catalyst amount from 0.05 to 0.1 g at 4 h of run time. Figure 12 depicts the influence of catalyst amount ranging from 0.05 to 0.2 g on the conversion at 343 K with EAcA to n-amyl alcohol molar ratio of 1:2 (Table 4). The increase in the concentration of the catalyst increases the number of active sites thereby enhancing the reaction rates. This implies that the basic strength as well as the density of basic sites is an important factor to accelerate transesterification. Further increase in the catalyst amount to 0.2 g showed no considerable change in the conversion, which suggests that 0.1 g of the catalyst would be adequate to carry out the reaction under the similar reaction conditions.

Figure 13 depicts the effect of molar ratio on the conversion of EAcA. With decrease in the molar ratio of EAcA to alcohol from 2:1 to 1:1, the conversion increased considerably from 62% to 92 %. Varying the molar ratio to 1:2 enhanced the conversion to 97 %. However negligible change was observed on further decrease in the molar ratio to 1:3 under similar reaction conditions. With excess alcohol concentration there may be preferential adsorption of alcohol rather than the ester thereby limiting the possibility of efficient collision between the ester and the alcohol and instead may facilitate many ineffective collisions between the alcohols alone. Hence 1:2 molar ratio of substrate to alcohol can be chosen as the optimum molar ratio.

Table 4 Effect of temperature and catalyst amount in the transesterificationof EAcA over CeAM catalyst. Time=4h, EAcA:n-amyl alcohol=1:2

Catalyst amount = 0.1 g T = 343 K

Temperature (K)	Conversion (%)	Catalyst amount (g)	Conversion (%)

313	38	0.05	85
323	43	0.1	97
333	77	0.2	98
343	97		

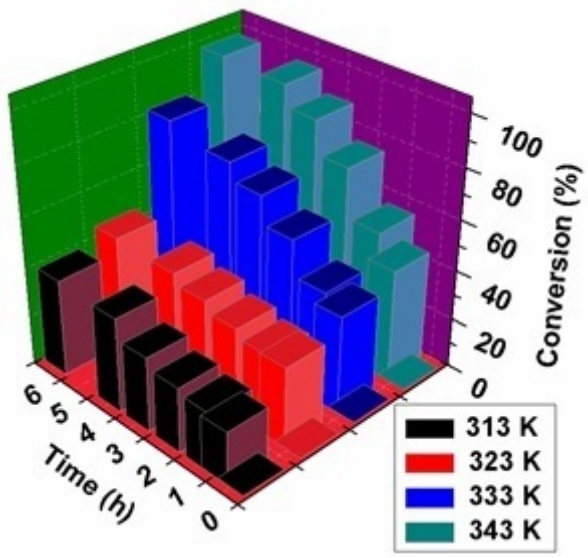

Figure 11. Effect of reaction temperature on the conversion.

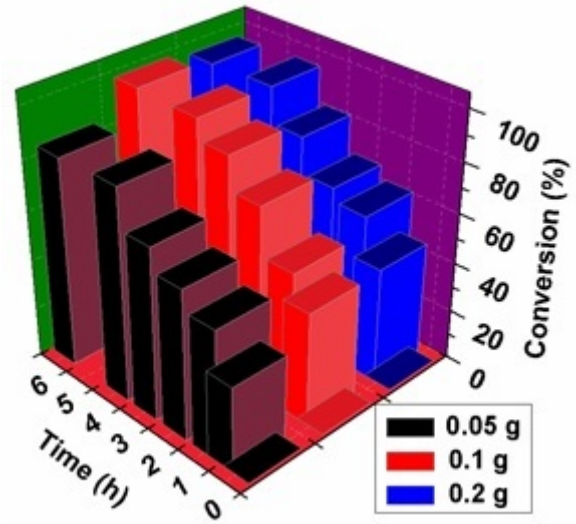

Figure 12. Effect of catalyst amount on the conversion.

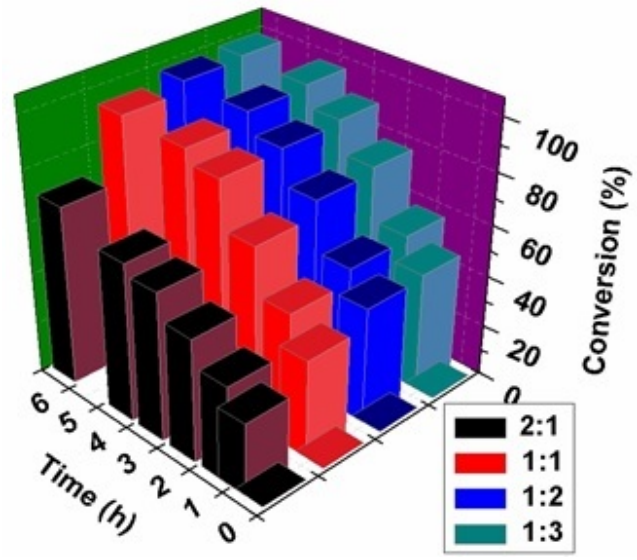

Figure 13. Effect of molar ratio on the conversion

Kinetics

The kinetic investigation of the transesterification reaction of EAcA with n-amyl alcohol was carried out based on experimental data under the optimum reaction conditions at different temperatures. The aim of the kinetic experiment was to resolve the overall order and rate constant (k) of the heterogeneous reaction. The general integrated rate expression for a second order heterogenous catalysed reaction is give by,

$$\frac{-dA}{dt} = kw[P][Q]$$

where [P], [Q] are the concentration of EAcA and n-amyl alcohol in molL^{-1} respectively and w is the weight of catalyst in g. Fogler model for a molar ratio, M=[QO]/[PO] ≠ 1, the above expression in terms of fractional conversion () of P can be expressed as [41],

$$ln\frac{M - X_P}{M\left[1 - X_P\right]} = \left[P_O\right][M - 1]kwt$$

$$X_P = \frac{\left[P_O\right] - [P]}{\left[P_O\right]}$$

where [PO] and [QO] are the initial concentration of the reactants. To examine the order of the reaction, ln{(M-XP)/ M(1-XP)} was plotted against time (Figure 14) at different temperatures and the results were observed to fit well for a second order reaction with acceptable R2 values (Table 5). The rate constants at different temperatures have been evaluated from the slope of the corresponding curve and are presented in Table 5. The rate constants is found to increase with incresing temperature and at 343 K the rate constant is calculated to be 9.13 × 10^{-2} L mol^{-1} min^{-1}. This is in good agreement with that examined by Rima et al.8 showing second order kinetics for transesterification of EAcA and n-butyl alcohol at 383 K. The efficiency in the fuctioning of catalytic reaction than that of a non-catalytic one depends mostly in the activation energy. The activation energy as calculated from the slope of Arrhenius plot (Figure 15) under similar reaction conditions and with CeAM catalyst is found to be 44 kJmol^{-1}.

Table 5. Rate constants at different temperatures

Temperature (K)	k (L mol^{-1} min^{-1})	R2
313	9.7 ´ 10-3	0.9
323	1.2´ 10-2	0.88
333	3.6 ´ 10-2	0.95

343	9.1 ´ 10-2	0.97

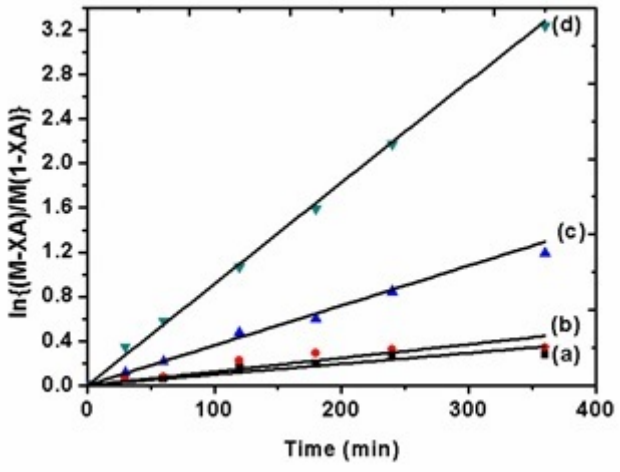

Figure 14. Linear fit for determining order of the rection at (a) 313 (b) 323 (c) 333 (d) 343 K

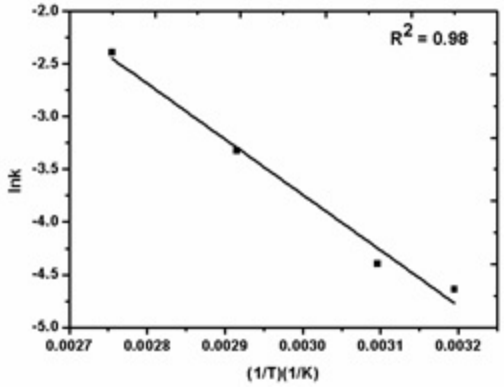

Figure 15. Arrhenius plot for determining the activation energy

Based on the mechanism proposed by Hattori et al. [42] and from above kinetic and experimental data a schematic mechanism may be proposed (scheme 2) for the present transesterification reaction. The catalytic cycle starts with the adsorption of the alcohol on the catalyst surface and is dissociated by coordinatively unsaturated Lewis acid- base pair site on ceria to produce alkoxy species on lewis acid site (Ce_4^+) and H^+ on lewis base site (O_2^-). Lamotte and his co-workers also confirmed the formation of methoxy species by FTIR experiments for adsorption of methanol on CeO_2 [43]. This is then followed by adsorption of EAcA at the neighbouring catalytic site. The carbonyl group of EAcA adsorbed over ceria results in polarization of C=O group and more positive charge is created over the carbonyl carbon. The next step involves the nucleophilic attack of the adsorbed alkoxy species over carbonyl carbon at the adjacent adsorbed site to form surface intermediates, which further rearranges and the desired product is desorbed from the catalyst surface together with ethyl alcohol. The present study agrees to that of Hattori and his co-workers that the surface reaction step is the rate determining step and we suggest the catalytic reaction to follow Langmuir-Hinshelwood mechanism [42]. The Lewis acid-basic pair sites on ceria perhaps might accelerate the adsorption of both EAcA and alcohol. Moreover, CO_2 TPD of the ceria supported MFI analysed by Margandan et al showed to exhibit both Bronsted and Lewis basicity [44]. The high mobility of oxygen within the lattice structure of ceria that enables it to form and eliminate intrinsic defects might also contribute to its catalytic activity [45].

To test the utility of alkali treated MFI as support, a controlled experiment was carried out with both parent MFI supported ceria (CePM) and CeAM under the optimised reaction conditions. The ceria loaded hierarchical MFI showed better results than the parent one (Table 6, entry 3,4) which confirmed the contributions of composite pore system that accommodates comparatively more amount of ceria resulting in higher concentration sites and facilitates better accessibility to the active sites. The structure-property function relationship between creation of mesoporosity in zeolite and catalytic activity of the same was proved by several authors [46-47] and we believe that the hierarchy

topology definitely helps in our case also. Raja et al also noticed similar results for SrO nanoparticles encaptulatedmesoporous carbon and reported increased conversion with increasing pore diameter of the catalyst [7].

We explored the scope and limitations of different alcohols for the transesterification of EAcA under the optimised conditions using CeAM. As evidenced from Figure 18 CeAM was found to be effective for aliphatic, cyclic, aryl and for tertiary alcohol as well. The catalyst showed best performance for linear aliphatic alcohols and the variation in chain length seemed to affect the conversion of EAcA. Vinu et al. also reported similar dependence of chain length, bulkiness of the alcohol and electron delocalisation on the activity of the catalyst [6]. Among the aliphatic alcohols considered, 1- butanol was found to react faster than n-amyl alcohol and 1-octanol which probably may be due to the ease in diffusion of reactants and products depending on its chain length. The initial β-ketoester was almost completely converted to the desired product within 4h when reacted with 1-butanol and 97% and 92% with n-amyl alcohol and 1-octanol respectively under the optimised conditions. Cyclohexanol was found to react more efficiently than benzyl alcohol but less than that of the linear alcohols. Weitzman reported the difficulty to achieve tertiary β-ketoester from EAcA due to its high thermodynamic stability and high rate of product decomposition [48]. In our case, CeAM was found to be active for t-butyl alcohol with at least 53% conversion. The redox properties of ceria and the hierarchical topology of the zeolite together might account for the activity of CeAM. However the lower conversion as compared to other alcohols can be attributed to the steric factor that imposes restriction in the diffusion process thereby reducing the possibility of contact with the active sites.

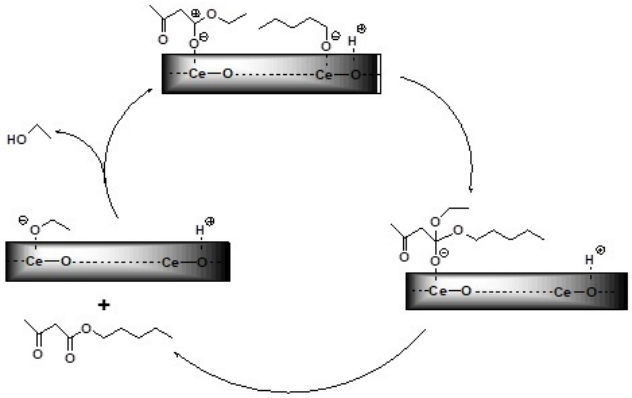

Scheme 2. Possible mechanism for the transesterification of ethyl acetoacetate with CeAM

Reaction conditions :EAcA:alcohol = 1:2, catalyst amount = 0.1 g, T = 343 K
Table 6. Transesterification of ethyl acetoacetate and different alcohols catalyzed by CeAM

Entry	Alcohols		Catalyst	Product		Conversion (%)
1			CeAM			100
2			CeAM			92
3			CeAM			97
4			CePM			85
5			CeAM			88
6			CeAM			82
7			CeAM			53

Reusability

To assess the heterogeneity of the catalyst, the EAcAtransesterification reaction was conducted using CeAM and n-amyl alcohol under the optimised conditions for 2h, and then the reaction was stopped. The catalyst was separated from the reaction mixture by filtration and reaction was continued further for 4, 6 and 8h. GC analysis showed no

progress in the reaction after removing the catalyst revealing the absence of catalyst leaching and proves the reaction to be truely heterogeneous. To verify the reusablity of the catalyst, another similar fresh reaction was performed for 4h. The catalyst was recovered by filtation, washed with acetone and dried in an oven at 383 K. Without further activation the catalyst was used for a series of recycling experiments under the optimised conditions. Figure 18 reveals that CeAM retained its activity on transesterification of EAcA even after the fifth repeated cycles.

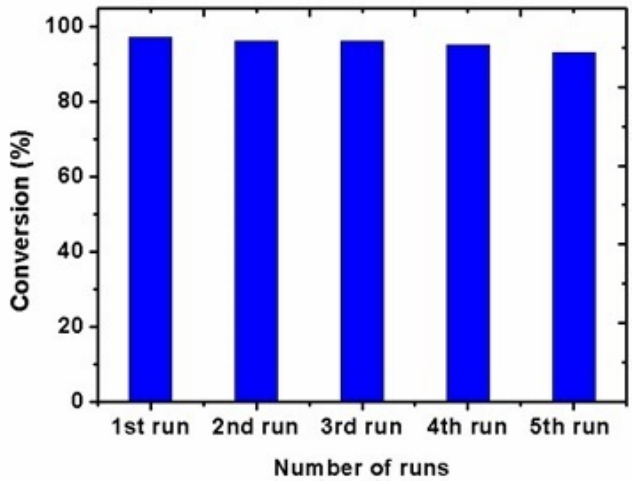

Figure 16. Reusability of the catalyst

CONCLUSION

We have shown that ceria loaded on hierarchical MFI is a very efficient catalyst for the transesterification of ethyl acetoacetate by n-amyl alcohol avoiding the usage of harmful solvents. The catalyst was also effective for cyclic, aryl and tertiary alcohols as well. The catalyst afforded a high yield of β-keto esters in a short reaction time and can be recycled for at least five times with retention of its catalytic activity. The excellent catalytic activity can be attributed to a combination of several factors such as presence of coordinatively unsaturated Lewis acid- base pair site on ceria, excellent crystallinity, high surface area and the hierarchical topology. The present scheme is very simple, convenient and could alleviate the problems of toxicity, corrosion, wastage, high expenses, thermal stability and catalyst reusability, that are being presently encountered by conventional homogenous catalysts.

ACKNOWLEDGEMENT

The authors are grateful to UGC for providing BSR fellowship to one of the author (MN). The authors also acknowledge the Department of Physics and Meterology, IIT Kharagpur, India for XPS analysis, SAIF, North-eastern Hill University for TEM analysis, IASST, Boragaon for XRD and SEM analysis, Department of Chemistry and Department of Instrumentation & USIC, Gauhati University for many necessary measurements associated with the present work.

REFERENCE

1. M H Zong, Z Q Duan, et al, *Green Chem*., **2007**, 9; p.434.
2. D Srinivas, R Srivastavaet al, *Catal. Today*,**2004**, 96; p.127.
3. JOtera, *Chem. Rev*.,**1993**, 93; 1449.
4. S Benetti, R Romagnoli, et al, *Chem. Rev*., **1995**, 95; p.1065.
5. CE Rehberg, CH Fischer, *J AmerChemSoc*, **1944**, 66; p.1203.
6. CAnand, S V Priya, et al, *Catal. Today*, **2013**, 204; p.164.
7. P K Raja, A Chokkalingam, et al, *J. Nanosci. Nanotechnol*., **2012**, 12; p.8467.
8. R Das, D Chakraborty, *Appl. Organometal. Chem*., **2012**, 26; p.140.